THE JOURNAL OF BIOLOGICAL CHEMISTRY VOL. 283, NO. 8, pp. 4520–4527, February 22, 2008

Mechanism, Regulation, and Functional Properties of *Dictyostelium* Myosin-1B*

Received for publication, September 28, 2007, and in revised form, November 21, 2007 Published, JBC Papers in Press, December 17, 2007, DOI 10.1074/jbc.M708113200

Georgios Tsiavaliaris[‡1], Setsuko Fujita-Becker[§], Ulrike Dürrwang[§], Ralph P. Diensthuber[‡], Michael A. Geeves[¶], and Dietmar J. Manstein[‡§]

From the [‡]Institute for Biophysical Chemistry, OE 4350, Hannover Medical School, Carl-Neuberg-Strasse 1, D-30623 Hannover, Germany, the [§]Department of Biophysics, Max Planck Institute for Medical Research, Jahnstrasse 29, D-69120 Heidelberg, Germany, and the [¶]Department of Biosciences, University of Kent, Canterbury CT2 7NJ, United Kingdom

Myosin-1B is one of three long tailed class-1 myosins containing an ATP-insensitive actin-binding site in the tail region that are produced in *Dictyostelium discoideum*. Myosin-1B localizes to actin-rich structures at the leading edge of migrating cells where it has been implicated in the formation and retraction of membrane projections, the recycling of plasma membrane components, and intracellular particle transport. Here, we have used a combination of molecular engineering approaches to describe the kinetic and motile properties of the myosin-1B motor and its regulation by TEDS site phosphorylation. Our results show that myosin-1B is a low duty ratio motor and displays the fastest nucleotide binding kinetics of any of the *Dictyostelium* class-1 myosins studied so far. Different from *Dictyostelium* myosin-1D and myosin-1E, dephosphorylated myosin-1B is not inactivated but moves actin filaments efficiently, albeit at an up to 8-fold slower velocity in the *in vitro* motility assay. A further difference is that myosin-1B lacks the ability to switch between rapid movement and bearing tension upon physiological changes of free Mg^{2+} ions. In this respect, its motor properties appear to be more closely related to *Dictyostelium* myosin-2 and rabbit skeletal muscle myosin.

The monomeric, non-filamentous class-1 myosins are among the most prevalent and most widely expressed myosins. The conserved N-terminal motor domain of class-1 myosins, which contains the ATP- and actin-binding sites, is followed by 1–6 light chain binding IQ motifs and more diverse C-terminal tail regions. Because of their diversity, the class-1 myosins can be further divided into at least four subclasses (1). The eukaryotic model system *Dictyostelium discoideum* has been used extensively to study the cellular functions of class-1 myosins (2–6). Seven class-1 myosins, Myosin-1A-F and Myosin-1K, are produced in *D. discoideum*. Myosin-1K completely lacks a tail region and has a large insert in the motor domain (7, 8). The *myoA*, *myoE*, and *myoF* gene products encode subfamily members with "short" tails that consist solely of a tail homology 1 (TH1) domain that interacts with anionic phospholipids and thereby binds to membranes. The *myoB*, *myoC*, and *myoD* gene products have "longer" tails that consist of a TH1 domain, a TH2 domain that is typically rich in the amino acids glycine, proline, alanine, or glutamine(GPA/Q) and binds actin in a ATP-insensitive manner, and an Src homology 3 (SH3) domain, which is known to mediate protein-protein interactions. Myosin-1 SH3 domains are usually referred to as TH3, to distinguish them from SH3-like domains found at the N terminus of other myosins.

Distinct, yet overlapping, roles for the *D. discoideum* class-1 myosins in actin-based cellular processes like endocytosis and cell movement were revealed by the defects of knock-out cells lacking single or multiple myosin-1 genes and cellular localization studies (9–15). Myosin-1B was shown to associate with the plasma membrane during locomotion (16), the anterior pseudopod (2), and eupodia (17). Its interaction with the adapter protein CARMIL appears to play a crucial role in recruiting components of the Arp 2/3 actin polymerization machinery to the plasma membrane (18). Detailed characterization of myosin-1B null cells has shown that the protein plays a role in cellular translocation, the suppression of lateral pseudopod formation, and rapid intracellular particle motility (19). A unique feature of myosin-1B is that its neck region is decorated by a compact, single-domain protein with two EF-hand motifs that has a molecular mass of 8 kDa and binds Ca^{2+} with submicromolar affinity. The myosin-1B light chain is thus >2-fold smaller than most of the common four-EF-hand myosin light chains (20).

Here, we describe the kinetic and functional properties of the myosin-1B motor domain and compare them with those of *Dictyostelium* myosin-2, the closely related "long tailed" myosin-1D, and the more distantly related "short-tailed" myosin-1E. To facilitate the characterization of myosin-1B motor properties, the motor domain fragment was fused to an artificial lever arm consisting of two α-actinin repeats (21, 22). A motor domain construct without lever arm was used to determine steady-state and transient kinetic parameters. The terminology used (B698, B698-2R) refers to the site of motor domain truncation and 2R serves as abbreviation for the attachment of two α-actinin repeats to the motor domain. Titus and coworkers (23) have shown that regulation by TEDS site phosphorylation does not play a role in the localization of myosin-1B but is absolutely required for *in vivo* function. Following stimulation of a cell with chemoattractant, TEDS site phosphorylation-induced

* This work was supported by Deutsche Forschungsgemeinschaft Grants MA1081/11-1 (to D. J. M.) and TS 169/3-1 (to G. T.) and Wellcome Trust Grant 070021 (to M. A. G.). The costs of publication of this article were defrayed in part by the payment of page charges. This article must therefore be hereby marked "*advertisement*" in accordance with 18 U.S.C. Section 1734 solely to indicate this fact.

[1] To whom correspondence should be addressed. Tel.: 49-511-532-8591; Fax: 49-511-532-5966; E-mail: gtsiaval@bpc.mh-hannover.de.

increases in myosin-1B motor activity were found to contribute to the global extension of pseudopodia that occurs prior to polarization and directed motility (24). To study the effects of TEDS site phosphorylation on the motor properties of the protein, we generated the dephosphorylated and phosphorylated forms of B698-2R by treatment with λ-phosphatase and *Acanthamoeba castellanii* myosin-I heavy chain kinase (25). Additionally, we generated mutant versions of B698-2R, which facilitated the combined characterization of motor and kinetic properties. The serine at the TEDS site of these constructs was replaced by either an alanine residue, to mimic the unphosphorylated state, or a glutamate residue, to mimic the phosphorylated state (15, 26–28). These constructs are referred to as S332A or S332E mutants in the following text.

EXPERIMENTAL PROCEDURES

Reagents—Standard chemicals were purchased from Sigma, and restriction enzymes, polymerases, and DNA-modifying enzymes were from Roche Applied Science. TRITC[2]-labeled phalloidin was a gift from Dr. H. Faulstich (29).

Plasmid Constructs and Mutagenesis—Genomic DNA was isolated from AX2 cells according to Ref. 30. PCR-directed mutagenesis was used to isolate a *myoB* gene fragment encoding the motor domain with a unique BamHI site at the 5′-end of the coding region and a unique XhoI site following the codon for residue 698. The PCR products were digested with BamHI and XhoI and cloned into pDXA-3H (31), which carries sequences for the fusion of a C-terminal His_8 tag. TEDS site mutants were generated by PCR-directed mutagenesis. The resulting plasmids were confirmed by sequencing. For the production of motor domain constructs fused to two *D. discoideum* α-actinin repeats (2R), a His_8 tag was obtained as XhoI/SphI fragment from pDH20-2R (32) and inserted in the XhoI/SphI-digested myosin-1B motor domain expression plasmid.

Protein Expression and Purification—*Dictyostelium* cells were grown in HL-5C medium (33). Cells were transformed by electroporation (34). G418 was used as selectable marker at 10 μg/μl. The myosin-1 constructs were purified as described previously for myosin-2 head fragments (28). Rabbit actin was purified by the method of Lehrer and Kerwar (35).

Direct Functional Assays—Actin sliding motility was measured as described previously (28, 36). TEDS site phosphorylation was performed by mixing 1 mg/ml B698-2R with 0.027 mg/ml activated *A. castellanii* myosin-I heavy chain kinase and incubation in the presence of 1 mM EGTA, 3 mM $MgCl_2$, and 2 mM ATP at 30 °C for 20 min. Myosin-I heavy chain kinase was activated by autophosphorylation at 30 °C for 20 min in a buffer containing 100 mM imidazole, pH 7.0, 4 mM ATP, 6 mM $MgCl_2$, and 2 mM EGTA (37). Myosin-I heavy chain kinase was generously provided by Drs. E. D. Korn and H. Brzeska (Laboratory of Cell Biology, NHLBI, National Institutes of Health). Dephosphorylation was performed by incubation of 1 mg/ml B698-2R with 4000 units/ml λ-protein phosphatase in the presence of 4 mM dithiothreitol, 2 mM $MnCl_2$, and 0.01% Brij 35 at 30 °C for 30 min.

$$M + ATP \underset{k_{-1}}{\overset{k_{+1}}{\rightleftharpoons}} M{\cdot}ATP \underset{k_{-2}}{\overset{k_{+2}}{\rightleftharpoons}} M^{*}{\cdot}ATP \underset{k_{-3}}{\overset{k_{+3}}{\rightleftharpoons}} M^{**}{\cdot}ADP{\cdot}P_i$$

$$\underset{k_{-4}}{\overset{k_{+4}}{\rightleftharpoons}} M^{*}{\cdot}ADP{\cdot}P_i \underset{k_{-5}}{\overset{k_{+5}}{\rightleftharpoons}} M^{*}{\cdot}ADP + P_i \underset{k_{-6}}{\overset{k_{+6}}{\rightleftharpoons}} M{\cdot}ADP \underset{k_{-7}}{\overset{k_{+7}}{\rightleftharpoons}} M + ADP$$

SCHEME 1. **7-step model of the interaction of myosin with nucleotides (41).**

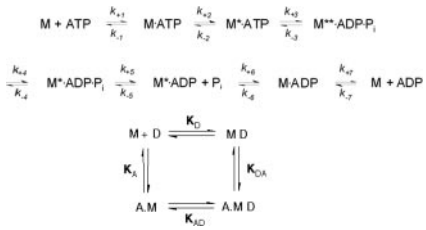

SCHEME 2. **Coupling between nucleotide and actin binding sites.**

Kinetic Measurements—Stopped-flow measurements were performed at 20 °C with a Hi-tech Scientific SF-61 DX2 double mixing stopped-flow system and an Applied Photophysics PiStar Instrument using procedures and kinetic models described previously (38–40). Binding and hydrolysis of ATP by myosin-1B head fragments were analyzed in terms of the seven-step model (see Scheme 1) described by Bagshaw *et al.* (41). Transients in the presence of actin were analyzed according to the mechanism described in Schemes 2 and 3 (42, 43). In these schemes a notation is used that distinguishes between the constants in the presence and absence of actin by using bold ($\mathbf{k_{-1}}$, $\mathbf{K_1}$) *versus* italic type (k_{-1}, K_1); subscript A and D refer to actin ($\mathbf{K_A}$) and ADP (K_D), respectively. The transient kinetics data were interpreted as described previously (28, 32, 38, 39, 44). Steady-state ATPase activities were measured at 25 °C with the NADH-coupled assay (44) in a buffer containing 25 mM HEPES, 25 mM KCl, and 4 mM $MgCl_2$. The myosin concentration was 0.25–1 μM. NADH oxidation was followed using the change in absorption at 340 nm in a Beckman DU-800 spectrophotometer.

RESULTS

Actin Activation of Myosin-1B ATPase Activity—To determine the maximum values of the ATPase activity and the efficiency of coupling between actin and nucleotide binding, we measured the ATPase rates with actin concentrations in the range of 0 to 60 μM F-actin (Fig. 1). At concentrations of actin much lower than K_{app}, the dependence of the apparent ATPase rate on actin concentration can be fitted to a straight line and the apparent second order rate constant (k_{cat}/K_{app}) of the reaction can be determined from the slope of this line. Estimates of K_{app} and k_{cat} were obtained from double reciprocal plots (Table 1), but as the maximum actin concentrations accessible are below the estimated value of K_{app} the values must be treated with some caution. Myosin-1B resembles in this respect *Dictyostelium* myosin-2 and myosin-1D, whereas chicken myosin-5a displays a much higher affinity for F-actin in the presence of ATP. The steady-state parameters are summarized in Table 1,

[2] The abbreviations used are: TRITC, tetramethylrhodamine isothiocyanate; LCBD, light chain binding domain; MOPS, 4-morpholinepropanesulfonic acid.

together with the published values for *Dictyostelium* myosin-1D, myosin-1E, and myosin 2. The ATPase activity of the S332A mutant of B698 is only slightly activated by the addition of 20 μM F-actin. The ATPase activity of the S332E mutant showed a hyperbolic dependence on actin concentration. Additionally, the coupling efficiency between actin and nucleotide binding is 16-fold tighter for the B698 Ser-to-Glu mutant than for the Ser-to-Ala mutant. A similar 20-fold change in k_{cat}/K_{app} was observed for the phosphorylated and dephosphorylated forms of *Acanthamoeba* myosin-1C (45), whereas the observed changes in k_{cat}/K_{app} are larger for *Dictyostelium* myosin-1D and myosin-1E with 77- and 170-fold increases for the phosphorylated forms.

Binding of Nucleotide to Myosin-1B—The rate constants measured for nucleotide binding to the wild-type forms of B698 and both TEDS site mutants were identical. Therefore, the data shown in Table 2 refer only to B698, although all measurements were performed with wild-type and both mutant constructs. The rate of ATP binding (K_1k_{+2}) could be monitored from the increase in intrinsic protein fluorescence following the addition of excess ATP. The increase in fluorescence for ATP binding is 4% for myosin-1B. In contrast, the increase in intrinsic protein fluorescence following the addition of excess ADP was too small to measure the rate of ADP binding (k_{-6}/K_7) reliably. Myosin-1B has seven Trp residues in the motor domain, including the conserved Trp in the relay loop that reports the open to closed transition of switch-2 that accompanies ATP hydrolysis (46). As most of them do not contribute to the signal change, this explains the small amplitude of the fluorescence change. As an alternative, the binding of the nucleotide analogues mantATP and mantADP was measured following the fluorescence enhancement after mixing with the myosin constructs. The results of these measurements were analyzed as described previously (32, 47) and are summarized in Table 2. The apparent second order association rate constants (K_1k_{+2} or k_{-6}/K_7) are similar for ATP and the mantADP and ATP analogues. The intrinsic fluorescence amplitude was too small to allow the maximum to be estimated, but k_{obs} displayed a linear dependence on ATP concentration up to observed rates of 100 s^{-1}. For most myosins the maximum rate constant has been attributed to the rate constant for the ATP hydrolysis step ($k_{+3} + k_{-3}$), which is signaled by the fluorescence change of the Trp located at the tip of the relay loop (47). These values are very high compared with most myosins and are comparable with those of myosin-5 (48). As ATP binding to B698 produced a larger fluorescence increase than the binding of ADP, the displacement of ADP by ATP could be followed from the net increase in fluorescence upon addition of a large excess of ATP to ADP-saturated B698. The rate of ADP release (k_{+6}) from B698 was 0.70 s^{-1}.

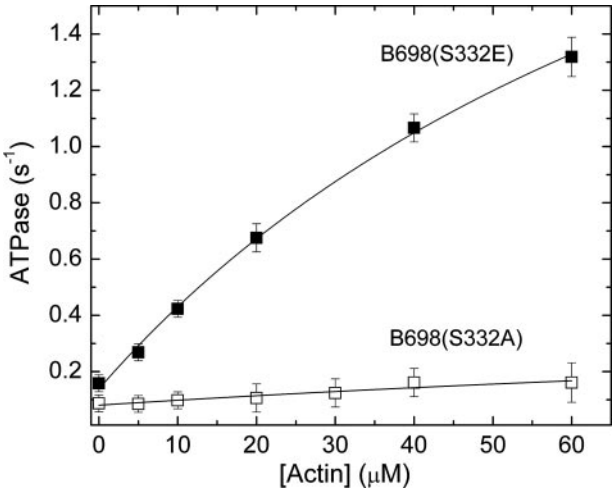

FIGURE 1. **Actin-activated ATPase activity.** Shown are the ATP turnover rates of B698(S332E) (■) and B698(S332A) (□) at increasing concentrations of F-actin. The observed rates were plotted against F-actin concentration and fitted to a hyperbola, giving the Michaelis parameters summarized in Table 1.

TEDS Site Phosphorylation of Myosin-1B Stabilizes the Actomyosin Complex—The rate of actin binding was measured following the exponential decrease in pyrene fluorescence observed on binding of an excess of pyrene-actin to the myosin-1B constructs. The observed rate constants were plotted against pyrene-actin concentration, and k_{obs} values were linearly dependent upon actin concentration over the range studied. The second order rate constants of pyrene-actin binding ($\mathbf{k_{+A}}$) were obtained from the slope of the plot, and the resulting values are summarized in Table 2. The $\mathbf{k_{+A}}$ values were unaffected by the TEDS site mutations S332A and S332E. In addition, the rate constant for actin dissociation ($\mathbf{k_{-A}}$)

TABLE 1
Actin activation of ATPase activity

Experimental conditions were 25 mM HEPES, pH 7.4, 25 mM KCl, 4 mM $MgCl_2$. Temperature, 25 °C. ND, not determined.

Myosin construct	ATPase activity[a]			Michaelis-Menten parameters[b,c]		
	Basal	Activated	Activation[d]	k_{cat}	K_{app}	k_{cat}/K_{app}
	s^{-1}	s^{-1}		s^{-1}	μM	$\mu M^{-1}\,s^{-1}$
B698(S332A)	0.09 ± 0.01	0.11 ± 0.02	0.2	ND	ND	0.002 ± 0.001
B698(S332E)	0.16 ± 0.02	0.68 ± 0.07	3.3	3.1 ± 0.4	96 ± 20	0.032 ± 0.006
D692(S332A)[e]	0.09 ± 0.01	0.10 ± 0.02	0.1	ND	ND	0.001 ± 0.0003
D692(S332E)[e]	0.10 ± 0.02	1.34 ± 0.10	12.4	10.0 ± 3.0	130 ± 50	0.077 ± 0.02
E698(S336A)[f]	0.04 ± 0.01	0.10 ± 0.05	1.5	n.d.	ND	0.001 ± 0.0002
E698(S336E)[f]	0.08 ± 0.01	2.50 ± 0.20	30.3	15.4 ± 5.0	91 ± 30	0.170 ± 0.03
M765[g]	0.08 ± 0.01	0.68 ± 0.09	7.5	2.6 ± 0.4	73 ± 20	0.036 ± 0.005

[a] Actin-activated ATPase activity was measured in the presence of 20 μM rabbit skeletal muscle F-actin.
[b] Values for k_{cat} and K_{app} were calculated from fitting the data to the Michaelis-Menten equation.
[c] The apparent second order rate constant for actin binding (k_{cat}/K_{app}) was obtained from the calculated ratio of both values. Alternatively, the data at concentrations of actin much lower than K_{app} could be fit to a straight line, and k_{cat}/K_{app} was determined from the slope of this line.
[d] ATPase activation = (actin-activated ATPase − basal ATPase)/basal ATPase.
[e] Ref. 28.
[f] Ref. 15.
[g] Ref. 36.

TABLE 2

Rate and equilibrium constants of the myosin and actomyosin ATPase cycle

Experimental conditions were 20 mM MOPS, pH 7.0, 5 mM $MgCl_2$, 100 mM KCl, 20 °C. ND, not determined; n.a., not applicable.

Nucleotide	Rate constant	B698	D692[a]	E698[b]	M765[c]
Nucleotide binding to M					
ATP	K_1k_{+2} (μM^{-1} s^{-1})	1.97 ± 0.01	0.66 ± 0.01	0.96 ± 0.03	0.70 ± 0.03
	k_{max} (s^{-1})	>1000	640 ± 10	900 ± 30	28 ± 4
MantATP	K_1k_{+2} (μM^{-1} s^{-1})	1.30 ± 0.02	0.53 ± 0.02	0.91 ± 0.01	0.81 ± 0.02
ADP	k_{-6}/K_7 (μM^{-1} s^{-1})	n. a.	0.98 ± 0.02	0.34 ± 0.02	n. a.
	k_{+6} (s^{-1})	0.70 ± 0.003	0.60 ± 0.002	3.13 ± 0.03	n. a.
	K_D (μM)	0.40 ± 0.10	1.8 ± 0.3	7.1 ± 0.4	7.0 ± 1
MantADP	k_{-6}/K_7 (μM^{-1} s^{-1})	1.48 ± 0.01	0.87 ± 0.01	0.79 ± 0.01	0.36 ± 0.004
Nucleotide binding to A·M					
ATP	$\mathbf{K_1k_{+2}}$ (μM^{-1} s^{-1})	1.11 ± 0.03	0.49 ± 0.01	0.40 ± 0.002	0.57 ± 0.04
	$\mathbf{k_{+2}}$ (s^{-1})	>700 ± 100	960 ± 20	750 ± 20	490 ± 20
ADP	$\mathbf{k_{+AD}}$ (μM^{-1} s^{-1})[d]	4.95 ± 0.5	ND	2.5 ± 0.5	>0.5
	$\mathbf{k_{-AD}}$ (s^{-1})	233 ± 20	ND	28 ± 4	>100
	$\mathbf{K_{AD}}$ (μM)[e]	47 ± 5	75 ± 4	12 ± 2	182 ± 28
	$\mathbf{K_{AD}}/K_D$[e]	118 ± 20	42 ± 8	1.7 ± 0.5	26 ± 3
	$\mathbf{K_{AD}}$ (μM)[f]	118 ± 30	140 ± 10	ND	n.a.
	$\mathbf{K_{AD}}/K_D$[f]	295 ± 30	78 ± 14	ND	n.a.

[a] Ref. 28.
[b] Ref. 15.
[c] Ref. 36.
[d] Calculated from $\mathbf{k_{+AD} = k_{-AD}/K_{AD}}$.
[e] Values refer to the Ser-to-Glu mutants of the myosin-1 motor domain constructs.
[f] Values refer to the Ser-to-Ala mutants.

was determined directly by chasing pyrene-actin with a 20-fold excess of unlabeled actin (Fig. 2). The observed process could be fit to a single exponential where k_{obs} corresponds directly to $\mathbf{k_{-A}}$. In contrast to similar rates of actin binding, actin dissociates 12 times faster from the Ser–to-Ala mutant than from the Ser-to-Glu mutant (Fig. 2, *inset*). The dissociation equilibrium constant ($\mathbf{K_A}$) for actin binding is calculated from the ratio of $\mathbf{k_{-A}}$ and $\mathbf{k_{+A}}$. The slower dissociation rate of the actomyosin complex results in a 12-fold higher actin affinity for the pseudo-phosphorylated S332E mutant.

ATP-induced Dissociation of Actomyosin—The binding of ATP to the actomyosin complex could be followed by observing the exponential increase in fluorescence of pyrene-actin as the complex dissociates following addition of excess ATP. Fluorescence transients were best fit to single exponentials at all ATP concentrations examined. The observed rate constants were linearly dependent upon ATP concentration in the range of 5 to 25 μM. The rate constants measured for nucleotide binding to the actomyosin complexes formed by the wild-type forms of B698 and both TEDS site mutants show small but significant differences. Unless otherwise stated, the values given in Table 2 correspond to the myosin-I heavy chain kinase-treated wild-type construct. The mechanism of ATP-induced fluorescence enhancement was modeled according to Scheme 3.

$$A \cdot M + ATP \underset{}{\overset{K_1}{\rightleftharpoons}} A \cdot M \cdot ATP \xrightarrow{k_{+2}} A + M \cdot ATP$$

SCHEME 3

The apparent second order binding constant $\boldsymbol{K_1k_{+2}}$, defined by the gradient of the plot, was 1.1 $\mu M^{-1}s^{-1}$ for S332E and 1.5 $\mu M^{-1}s^{-1}$ for S332A. At high ATP concentrations (>2 mM) the observed rate constants saturated for the S332E mutant and the dependence on the ATP concentration could be described by a hyperbola, where the maximum value of k_{obs} defines $\boldsymbol{k_{+2}}$ (Table 2). For S332A the ATP-induced actin dissociation kinetics could be followed up to 600 μM ATP. At higher ATP concentrations the dissociation kinetics could not be resolved further due to the progressively weaker intensity of the fluorescence signal (data not shown).

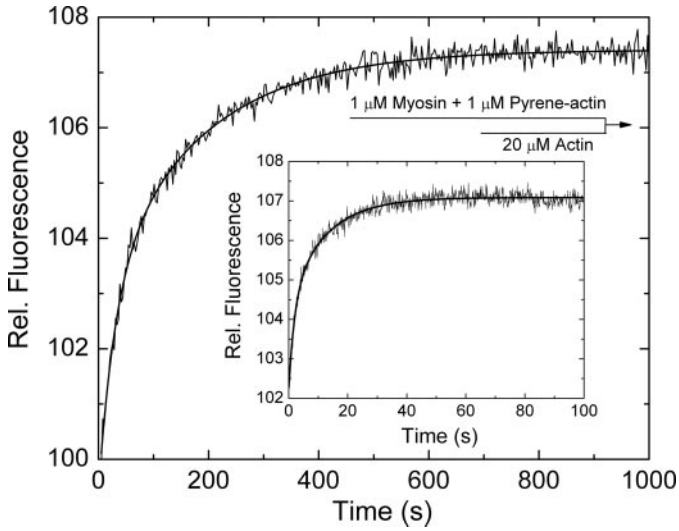

FIGURE 2. **Rates of pyrene-actin dissociation from B698(S332E) and B698(S332A) (*inset*).** The dissociation rate constant of actin ($\mathbf{k_{-A}}$) was determined from the rate of fluorescence enhancement that follows the addition of an excess of unlabeled F-actin to a sample of pyrene-labeled F-actin equilibrated with an equimolar amount of the myosin-1B constructs. B698(S332A) displays a 34-fold faster actin dissociation reaction than the B698(S332E) mutant. The concentrations shown in the mixing scheme refer to the concentrations of the reactants after mixing in the stopped-flow observation cell. The observed changes in fluorescence intensity are best fit by double exponentials. We attribute the fast first phase to a displacement reaction caused by small concentrations of ADP that are present in the F-actin solution.

Competitive Binding of ATP and ADP to Actomyosin—The affinity of ADP for the actomyosin complex ($\mathbf{K_{AD}}$) was determined from the inhibition of the ATP-induced dissociation of actomyosin by ADP. The observed rate of dissociation was reduced for all constructs when excess ATP was added to actomyosin in the pres-

ence of varying concentrations of ADP. The reaction was monophasic (Fig. 3). The observed rate constants were plotted against the ADP concentration, and the data were fitted with a hyperbola (Fig. 3). A dissociation equilibrium constant ($\mathbf{K_{AD}}$) of 47 μM was obtained for the B698(S332E) construct and 118 μM for the B698(S332A) construct. For comparison $\mathbf{K_{AD}}$ for D692(S332E) was 75 and 12 μM for E698(S336E). In accordance with thermodynamic consistency, the equilibrium constant for actin in the presence of ADP ($\mathbf{K_{DA}}$) was calculated as follows: $\mathbf{K_{DA}} = \mathbf{K_{AD}}/K_D \times \mathbf{K_A}$. In the presence of ADP, B698(S332E) displays a 66-fold higher affinity for actin than B698(S332A) (see Table 3).

TEDS Site Phosphorylation Increases the Motile Activity of Myosin-1B—The motor function of myosin-1B was analyzed measuring the gliding velocity of actin filaments in an *in vitro* motility assay (49). To investigate the regulation of myosin-1B by TEDS site phosphorylation, we treated the purified B698-2R construct with λ-phosphatase to generate the dephosphorylated form or with myosin-I heavy chain kinase (35) to generate the phosphorylated form. Additionally, we used B698-2R with the TEDS site mutations S332E or S332A to mimic the phosphorylated and dephosphorylated states of the protein. The movement of more than 100 filaments was followed and their velocity determined for each form of the B698-2R construct. The average sliding velocities are summarized in Table 4. The phosphorylated construct moved actin filaments 5.6 times faster than the dephosphorylated form. The Ser-to-Glu mutants of B698-2R displayed with 1.85 μm/s an 8.4 times faster velocity than the Ser-to-Ala mutant (Fig. 4). However, the motor activity of the myosin-1B S332A construct is significantly higher than observed with the equivalent myosin-1D and myosin-1E mutant constructs.

Previously, we observed that the concentration of free Mg^{2+} ions that is typically used in the *in vitro* motility assay has an inhibitory effect on the motile activity of *Dictyostelium* myosin-1D and myosin-1E (15, 28). Changes in total Mg^{2+} concentration in the range from 0.1 to 20 mM produced no change in the average sliding velocity of the myosin-1B constructs. In good agreement with this result, the value of $\mathbf{K_{AD}}$ was independent of changes in the concentration of free Mg^{2+} ions.

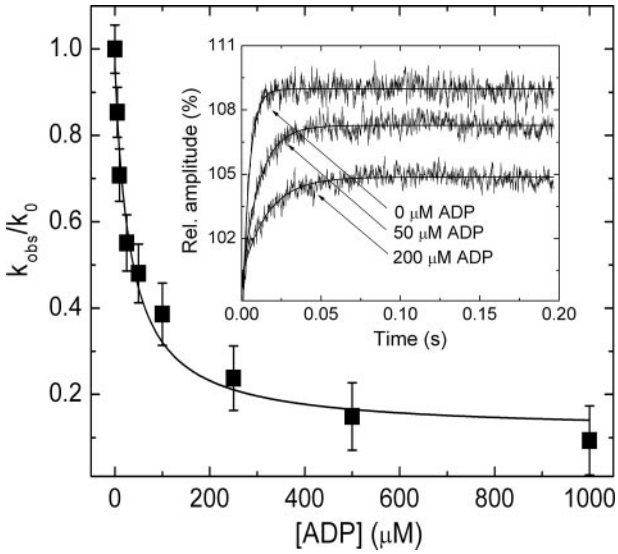

FIGURE 3. **ADP inhibition of the ATP-induced dissociation of the acto-B698(S332E) complex.** Monophasic ATP-induced dissociation reactions are observed in the absence and presence of micromolar concentrations of ADP. The observed amplitudes and rates decrease as more ADP is added (*inset*). A plot of the observed rate constants *versus* ADP concentration is shown. The data are fitted with a hyperbola resulting in a $\mathbf{K_{AD}}$ of 47 μM. *Error bars* represent standard deviations from at least 15 determinations of each data point.

DISCUSSION

Here we employ a molecular engineering approach to assess the motile activity of myosin-1B and its regulation. The approach of replacing the light chain binding domain (LCBD) with spectrin-like repeats acting as artificial lever arm has proved to be a very robust and widely applicable tool for the characterization of myosins from different classes and sources. As the motor domain-LCBD interface belongs to the most highly conserved regions of myosins and based on the atomic resolution structure of the myosin-2 motor domain with an artificial lever arm consisting of two α-actinin repeats, the functional linkage of motor domain and artificial lever arm is straightforward (15, 22, 28, 50–52). The resulting single polypeptide constructs can be produced with much better yields than constructs with a native LCBD. The lever arm length corresponds to 12 nm for the two α-actinin repeat constructs. When corrected for the differences in lever arm length, constructs with native LCBD and with artificial lever arm display identical motile activity (21, 52). The replacement of TEDS site Ser or Thr residues by Glu, Asp, or Ala residues, to generate the pseudo-phosphorylated or pseudo-dephosphorylated forms of the motor, was pioneered by the Korn laboratory (26) and has proved to be a valuable tool in studying regulation of myosin motor activity by TEDS site modification in studies addressing

TABLE 3
Actin affinities in the absence and presence of nucleotide
Experimental conditions for all measurements were 20 mM MOPS, 5 mM $MgCl_2$, 100 mM KCl, pH 7.0, 20 °C.

Myosin construct	k_{+A}	k_{-A}	K_A	K_{DA} (μM) = K_A*K_{AD}/K_D
	$\mu M^{-1} s^{-1}$	s^{-1}	nM	
B698[a]	1.1 ± 0.2	0.005 ± 0.0003	4.5 ± 1	0.53 ± 0.1
B698(S332A)	1.4 ± 0.2	0.160 ± 0.003	114 ± 3	33.6 ± 1.6
B698(S332E)	1.1 ± 0.1	0.0047 ± 0.001	4.3 ± 1	0.51 ± 0.04
D692(S332A)[b]	4.1 ± 0.3	0.087 ± 0.0019	21.2 ± 5	3.6 ± 0.8
D692(S332E)[b]	1.4 ± 0.1	0.0027 ± 0.0002	1.9 ± 0.3	0.008 ± 0.002
E698(S336E)[c]	2.9 ± 0.2	0.0015 ± 0.0001	0.5 ± 0.1	0.001 ± 0.0005
M765[d]	0.8 ± 0.1	0.0025 ± 0.0004	3.1 ± 0.5	0.080 ± 0.014

[a] Myosin-I heavy chain kinase-treated. Treatment of the myosin constructs with apyrase did not result in significant changes in the observed rate constants.
[b] Ref. 28.
[c] Ref. 15.
[d] Ref. 36.

TABLE 4

Sliding velocity of actin filaments

Experimental conditions were 2 mM ATP, 4 mM $MgCl_2$, 25 mM imidazole, pH 7.4, 25 mM KCl, 1 mM EGTA, 10 mM dithiothreitol, 30 °C. The average velocity of the myosin-2 construct M765-2R was 1.5 ± 0.1 μm/s under identical assay conditions.

	Average velocity[a]		
	B698-2R	D692-2R[b]	E698-2R[c]
	μm/s	μm/s	μm/s
λ-Phosphatase treated	0.23 ± 0.09	No motility	0.08 ± 0.03
Myosin-I heavy chain kinase-treated	1.29 ± 0.21	0.89 ± 0.10	0.42 ± 0.04
Ser-to-Ala	0.22 ± 0.12	0.05 ± 0.02	No motility
Ser-to-Glu	1.85 ± 0.19	0.67 ± 0.09	0.35 ± 0.06

[a] Uncertainties represent S.D. of the mean values.
[b] Ref. 28.
[c] Ref. 15.

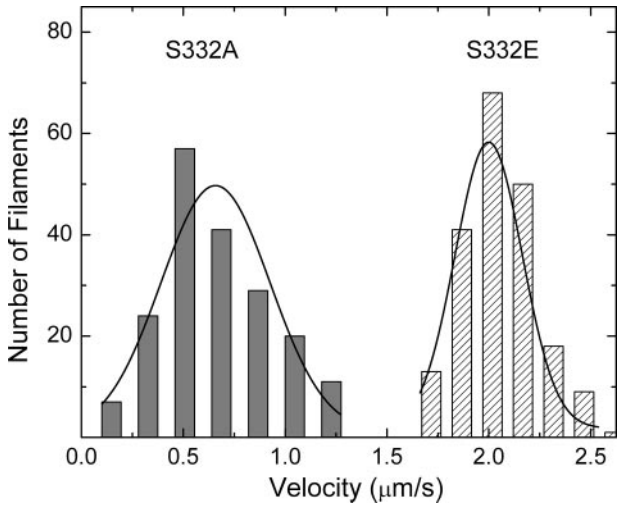

FIGURE 4. ***In vitro* motor activities.** Motor function was analyzed by measuring the sliding velocity of TRITC-labeled F-actin on myosin-coated surfaces under a fluorescence microscope (15). For each experiment, 0.2 mg/ml anti-His antibody-immobilized myosin, 20 nM TRITC-labeled F-actin, and 2 mM ATP were used. The movement of at least 100 filaments was followed, and the average sliding velocity was determined by the analysis of the Gaussian distribution. B698(S332A) (*gray bars*) moved actin filaments at 0.22 ± 0.12 μm/s and B698(S332E) (*cross-striped bars*) at 1.85 ± 0.19 μm/s at 30 °C.

myosins from several organisms and classes (15, 23, 27, 28, 53). In addition to examining the kinetic properties of the phosphorylated, dephosphorylated, pseudo-phosphorylated, and pseudo-dephosphorylated myosin-1B, the use of constructs that are equipped with an artificial lever arm and lack the tail region with its ATP-insensitive actin-binding site enabled us to directly study the motile properties of the myosin-1B motor and its regulation. Previous work on the kinetic and functional properties of *Dictyostelium* myosin-1D, myosin-1E, and myosin-2 constructs with an identical artificial lever arm allows us to directly compare the motile activity of three class-1 myosins from two different subgroups and of a class-2 non-muscle myosin (15, 28).

The rates of nucleotide binding to B698 and the apparent second order equilibrium constant in the absence (K_1k_{+2}) and presence ($\mathbf{K_1k_{+2}}$) of actin are faster than those measured for *Dictyostelium* myosin-2 and the other characterized class-1 myosins. In addition to displaying faster kinetics for ATP binding and ADP dissociation, myosin-1B shares with other class-1 myosins a Thr residue in the relay helix and an Asn residue in the Src homology 1 helix. Based on the structure of the myosin-1E motor domain, a hydrogen bond formed between both residues is predicted to induce a larger kinking of the relay helix, resulting in an up to 30° greater lever arm rotation than observed for myosin-2 (54). The faster nucleotide binding kinetics and a larger lever arm rotation are consistent with the more than 2-fold faster motile activity of this myosin compared with *Dictyostelium* myosin-2, myosin-1D, and myosin-1E.

In general, the kinetic properties displayed by the myosin-1B constructs are compatible with a motor that functions in the context of a crowded environment of actin bundles in concert with many motors of the same or a similar type. In this situation it is important to shorten the duration of the steps spent in strongly bound states and to have weak binding M-ATP and M-ADP-P_i states that allow hydrolysis and recovery stroke to occur while the motor is detached from actin. This is supported by the fact that myosin-1B displays a weaker affinity for actin in the presence of ADP in comparison with other myosins. Additionally, the difference in the $\mathbf{K_{DA}}$ values determined for phosphorylated and dephosphorylated myosin-1B is >5-fold smaller than observed with myosin-1D.

Similar to the results obtained in previous studies, our steady-state kinetic measurements demonstrate that the presence of a negative charge at the TEDS site increases the ability of F-actin to stimulate myosin-1B ATPase activity by strengthening the coupling between binding to F-actin and the release of inorganic phosphate. The results of the transient kinetics experiments show that charge changes at the TEDS site do not affect the interactions between the myosin motor and nucleotides but the presence of a negative charge is important to stabilize the actomyosin complex. This is due to a stabilization of bound F-actin by the 34-fold reduced actin off-rate ($\mathbf{k_{-A}}$). Similar effects were previously observed following the introduction of a single negative charge in the actin binding region of *Dictyostelium* myosin-2 (44). Both the maximum turnover rate (k_{cat}) and the coupling efficiency between actin and nucleotide binding (k_{cat}/K_{app}) are increased, although the changes are not as pronounced as observed with *Dictyostelium* myosin-1D and myosin-1E (15, 26, 28). Our results do further suggest that the dephosphorylated form of myosin-1B is a better motor than the dephosphorylated forms of the other class-1 myosins. The activated form of myosin-1B is a low duty ratio motor and is under unloaded conditions predominantly weakly bound or detached from actin. Dephosphorylation leads to a further reduction in the duty cycle but apparently not to the extent that local high concentrations of myosin-1B are unable to work as effective motors.

Our results show once more that the kinetic and functional properties of myosins do not generally correlate with the class, subclass, or species from which a myosin was isolated. The long-tailed myosin-1B and myosin-1D display a greater level of similarity in regard to their coupling ratio ($\mathbf{K_{AD}}/K_D$), 118 and 42 for the activated forms, respectively. The short-tailed myosin-1E has a coupling ratio of 1.7, which is due to a significantly weaker affinity for ADP in the absence of F-actin (K_D) and a higher affinity for ADP in the presence of F-actin ($\mathbf{K_{AD}}$). Myosin-1E is in this respect similar to brush-border myosin-1 and Myr1, which both have been shown to display an ADP-induced neck movement (55–57). It has been proposed that ADP release

may be very sensitive to the load on the motor domain of these myosins and that they are designed to carry large loads or to cross-link load-bearing actin filaments (58).

However, the short-tailed myosin-1E shares more similarities with the long-tailed myosin-1D in regard to the regulation of its motor activity. Myosin-1B lacks the ability, displayed by myosin-1D and myosin-1E, to switch between fast movement and an increased capacity for bearing tension upon physiological changes in the concentration of free Mg^{2+} ions. The actin sliding velocities of both myosin-1D and myosin-1E were shown to be affected by physiological changes in the concentration of free Mg^{2+} ions (15, 28). Increased levels of free Mg^{2+} ions inhibit the release of ADP from both myosins leading to the accumulation of the strong binding A·M·ADP intermediate. This results in a reduced ability to produce fast movement but increases their capacity for bearing tension. In contrast, inhibition of myosin-1B motility by free Mg^{2+} ions was not observed even in the presence of 10-fold higher concentrations of free Mg^{2+} ions. Myosin-1B resembles in this respect *Dictyostelium* myosin-2 and rabbit skeletal muscle myosin.

In conclusion, our results demonstrate the strength of the molecular engineering approach to replace the LCBD with artificial lever arm for the elucidation of the motor properties of myosins that are otherwise inaccessible to direct functional analysis of their motor activity, *e.g.* due to the presence of an ATP-insensitive actin-binding site in the tail region or the lack of detailed knowledge about the associated light chains. Myosin-1B displays distinct functional and regulatory properties. It acts as a low duty ratio motor and displays fast nucleotide binding kinetics, 2- to 4-fold faster motility than any of the other *Dictyostelium* myosins, and 6-fold changes in motile activity that are dependent on phosphorylation status of the TEDS site, and its ADP dissociation kinetics are not affected by physiological changes in the concentration of free Mg^{2+} ions. Finally, studies like this one confirm once more that kinetic and functional properties do not generally correlate with the class, subclass, or the species from which a protein is isolated. Together with structural studies, they form the basis and are an essential precondition for rational bioinformatics-based approaches to predict functional differences between related enzymes.

Acknowledgments—We thank S. Zimmermann, R. Schumann, and C. Wassmann for excellent technical assistance, E. D. Korn for providing A. castellanii myosin-I heavy chain kinase, and I. Chizhov and R. Fedorov for help and discussions.

REFERENCES

1. Gillespie, P. G., Albanesi, J. P., Bähler, M., Bement, W. M., Berg, J. S., Burgess, D. R., Burnside, B., Cheney, R. E., Corey, D. P., Coudrier, E., de Lanerolle, P., Hammer, J. A., Hasson, T., Holt, J. R., Hudspeth, A. J., Ikebe, M., Kendrick-Jones, J., Korn, E. D., Li, R., Mercer, J. A., Milligan, R. A., Mooseker, M. S., Ostap, E. M., Petit, C., Pollard, T. D., Sellers, J. R., Soldati, T., and Titus, M. A. (2001) *J. Cell Biol.* **155,** 703–704
2. Jung, G., Wu, X., and Hammer, J. A., III (1996) *J. Cell Biol.* **133,** 305–323
3. Falk, D. L., Wessels, D., Jenkins, L., Pham, T., Kuhl, S., Titus, M. A., and Soll, D. R. (2003) *J. Cell Sci.* **116,** 3985–3999
4. Neuhaus, E. M., and Soldati, T. (2000) *J. Cell Biol.* **150,** 1013–1026
5. Novak, K. D., Peterson, M. D., Reedy, M. C., and Titus, M. A. (1995) *J. Cell Biol.* **131,** 1205–1221
6. Wessels, D., Titus, M., and Soll, D. R. (1996) *Cell Motil. Cytoskeleton* **33,** 64–79
7. Schwarz, E. C., Geissler, H., and Soldati, T. (1999) *Cell Biochem. Biophys.* **30,** 413–435
8. Yazu, M., Adachi, H., and Sutoh, K. (1999) *Biochem. Biophys. Res. Commun.* **255,** 711–716
9. Jung, G., and Hammer, J. A., III (1990) *J. Cell Biol.* **110,** 1955–1964
10. Titus, M. A., Wessels, D., Spudich, J. A., and Soll, D. (1993) *Mol. Biol. Cell* **4,** 233–246
11. Jung, G., Fukui, Y., Martin, B., and Hammer, J. A., III (1993) *J. Biol. Chem.* **268,** 14981–14990
12. Peterson, M. D., Novak, K. D., Reedy, M. C., Ruman, J. I., and Titus, M. A. (1995) *J. Cell Sci.* **108,** 1093–1103
13. Novak, K. D., and Titus, M. A. (1997) *J. Cell Biol.* **136,** 633–647
14. Schwarz, E. C., Neuhaus, E. M., Kistler, C., Henkel, A. W., and Soldati, T. (2000) *J. Cell Sci.* **113,** 621–633
15. Dürrwang, U., Fujita-Becker, S., Erent, M., Kull, F. J., Tsiavaliaris, G., Geeves, M. A., and Manstein, D. J. (2006) *J. Cell Sci.* **119,** 550–558
16. Senda, S., Lee, S. F., Cote, G. P., and Titus, M. A. (2001) *J. Biol. Chem.* **276,** 2898–2904
17. Fukui, Y., and Inoue, S. (1997) *Cell Motil. Cytoskeleton* **36,** 339–354
18. Jung, G., Remmert, K., Wu, X., Volosky, J. M., and Hammer, J. A., III (2001) *J. Cell Biol.* **153,** 1479–1497
19. Wessels, D., Murray, J., Jung, G., Hammer, J. A., III, and Soll, D. R. (1991) *Cell Motil. Cytoskeleton* **20,** 301–315
20. Crawley, S. W., de la Roche, M. A., Lee, S. F., Li, Z., Chitayat, S., Smith, S. P., and Cote, G. P. (2006) *J. Biol. Chem.* **281,** 6307–6315
21. Anson, M., Geeves, M. A., Kurzawa, S. E., and Manstein, D. J. (1996) *EMBO J.* **15,** 6069–6074
22. Kliche, W., Fujita-Becker, S., Kollmar, M., Manstein, D. J., and Kull, F. J. (2001) *EMBO J.* **20,** 40–46
23. Novak, K. D., and Titus, M. A. (1998) *Mol. Biol. Cell* **9,** 75–88
24. Gliksman, N. R., Santoyo, G., Novak, K. D., and Titus, M. A. (2001) *J. Biol. Chem.* **276,** 5235–5239
25. Brzeska, H., and Korn, E. D. (1996) *J. Biol. Chem.* **271,** 16983–16986
26. Wang, Z. Y., Wang, F., Sellers, J. R., Korn, E. D., and Hammer, J. A., III (1998) *Proc. Natl. Acad. Sci. U. S. A.* **95,** 15200–15205
27. De La Cruz, E. M., Ostap, E. M., and Sweeney, H. L. (2001) *J. Biol. Chem.* **276,** 32373–32381
28. Fujita-Becker, S., Dürrwang, U., Erent, M., Clark, R. J., Geeves, M. A., and Manstein, D. J. (2005) *J. Biol. Chem.* **280,** 6064–6071
29. Faulstich, H., Trischmann, H., and Mayer, D. (1983) *Exp. Cell Res.* **144,** 73–82
30. Bain, G., and Tsang, A. (1991) *Mol. Gen. Genet.* **226,** 59–64
31. Manstein, D. J., Schuster, H. P., Morandini, P., and Hunt, D. M. (1995) *Gene* **162,** 129–134
32. Kurzawa, S. E., Manstein, D. J., and Geeves, M. A. (1997) *Biochemistry* **36,** 317–323
33. Furch, M., Remmel, B., Geeves, M. A., and Manstein, D. J. (2000) *Biochemistry* **39,** 11602–11608
34. de Hostos, E. L., Bradtke, B., Lottspeich, F., Guggenheim, R., and Gerisch, G. (1991) *EMBO J.* **10,** 4097–4104
35. Lehrer, S. S., and Kerwar, G. (1972) *Biochemistry* **11,** 1211–1217
36. Tsiavaliaris, G., Fujita-Becker, S., Batra, R., Levitsky, D. I., Kull, F. J., Geeves, M. A., and Manstein, D. J. (2002) *EMBO Rep.* **3,** 1099–1105
37. Brzeska, H., Young, R., Knaus, U., and Korn, E. D. (1999) *Proc. Natl. Acad. Sci. U. S. A.* **96,** 394–399
38. Cremo, C. R., and Geeves, M. A. (1998) *Biochemistry* **37,** 1969–1978
39. Batra, R., Geeves, M. A., and Manstein, D. J. (1999) *Biochemistry* **38,** 6126–6134
40. Furch, M., Fujita-Becker, S., Geeves, M. A., Holmes, K. C., and Manstein, D. J. (1999) *J. Mol. Biol.* **290,** 797–809
41. Bagshaw, C. R., Eccleston, J. F., Eckstein, F., Goody, R. S., Gutfreund, H., and Trentham, D. R. (1974) *Biochem. J.* **141,** 351–364
42. Siemankowski, R. F., and White, H. D. (1984) *J. Biol. Chem.* **259,** 5045–5053
43. Millar, N. C., and Geeves, M. A. (1983) *FEBS Lett.* **160,** 141–148
44. Furch, M., Geeves, M. A., and Manstein, D. J. (1998) *Biochemistry* **37,**

6317–6326
45. Ostap, E. M., Lin, T., Rosenfeld, S. S., and Tang, N. (2002) *Biochemistry* **41,** 12450–12456
46. Batra, R., and Manstein, D. J. (1999) *Biol. Chem.* **380,** 1017–1023
47. Woodward, S. K., Geeves, M. A., and Manstein, D. J. (1995) *Biochemistry* **34,** 16056–16064
48. De La Cruz, E. M., Wells, A. L., Rosenfeld, S. S., Ostap, E. M., and Sweeney, H. L. (1999) *Proc. Natl. Acad. Sci. U. S. A.* **96,** 13726–13731
49. Kron, S. J., and Spudich, J. A. (1986) *Proc. Natl. Acad. Sci. U. S. A.* **83,** 6272–6276
50. Hachikubo, Y., Ito, K., Schiefelbein, J., Manstein, D. J., and Yamamoto, K. (2007) *Plant Cell Physiol.* **48,** 886–891
51. Ito, K., Kashiyama, T., Shimada, K., Yamaguchi, A., Awata, J., Hachikubo, Y., Manstein, D. J., and Yamamoto, K. (2003) *Biochem. Biophys. Res. Commun.* **312,** 958–964
52. Ruff, C., Furch, M., Brenner, B., Manstein, D. J., and Meyhofer, E. (2001) *Nat. Struct. Biol.* **8,** 226–229
53. Oberholzer, U., Marcil, A., Leberer, E., Thomas, D. Y., and Whiteway, M. (2002) *Eukaryot. Cell* **1,** 213–228
54. Kollmar, M., Dürrwang, U., Kliche, W., Manstein, D. J., and Kull, F. J. (2002) *EMBO J.* **21,** 2517–2525
55. Jontes, J. D., and Milligan, R. A. (1997) *J. Cell Biol.* **139,** 683–693
56. Jontes, J. D., Wilson-Kubalek, E. M., and Milligan, R. A. (1995) *Nature* **378,** 751–753
57. Veigel, C., Coluccio, L. M., Jontes, J. D., Sparrow, J. C., Milligan, R. A., and Molloy, J. E. (1999) *Nature* **398,** 530–533
58. El Mezgueldi, M., Tang, N., Rosenfeld, S. S., and Ostap, E. M. (2002) *J. Biol. Chem.* **277,** 21514–21521